Signaling With Imperfect Channel State Information: A Battery Power Efficiency Comparison

Fengzhong Qu, *Student Member, IEEE*, Dongliang Duan, *Student Member, IEEE*, Liuqing Yang, *Senior Member, IEEE*, and Ananthram Swami, *Fellow, IEEE*

***Abstract*—Due to complexity considerations, pulse-based modulations such as pulse position modulation (PPM) and ON–OFF keying (OOK) are well suited for wireless sensor networks (WSNs) since they provide the possibility of carrier-less signaling and, more importantly, noncoherent reception bypassing channel estimation at the receiver. In this paper, we compare PPM and OOK in terms of their battery power efficiencies, using a nonlinear battery model, and under the same bandwidth occupancy, bandwidth efficiency and cutoff rate requirement. Cutoff rate is used as our comparison criterion because it leads to a tractable analysis that is often impossible through direct evaluation of random coding exponent or capacity. In addition, cutoff rate gives a universal expression for both coherent and noncoherent detection by simply setting various channel state information (CSI) qualities. Our system model integrates typical WSN transmission and reception modules with realistic nonlinear battery models. Circuit power consumption, dc–dc converter efficiency, and power amplifier efficiency are also taken into consideration. Our analytical results characterize the signal-to-noise ratio (SNR)–cutoff rate–CSI region where PPM is more power efficient than OOK, and vice versa. We provide an interpretation in terms of the transmission range and symbol set size. Numerical results are also provided to verify the analysis.**

***Index Terms*—Battery power efficiency (BPE), imperfect channel state information (CSI), ON–OFF keying (OOK) modulation, pulse-position modulation (PPM), wireless sensor networks (WSNs).**

I. Introduction

BATTERY power efficiency (BPE) is critical in wireless sensor networks (WSNs) since sensor nodes are often expected to operate unattended for a long period of time [1]. Among existing physical layer approaches to improve BPE, a majority (see, e.g., [2], [8], and [13]) assumes that the batteries are ideal and linear. In fact, however, part of the battery's capacity (stored energy) is always wasted during its discharge process, especially when the discharge current is large. Experiments show that the actual battery discharge is a *nonlinear* process [12], [16]. Linear battery models are unrealistic; incorporation of empirically derived realistic battery models has the potential to markedly improve system lifetime [7]. In [9], the BPEs of pulse position modulation (PPM) and frequency shift keying (FSK) were compared under the average symbol error rate (SER) bound criterion using nonlinear battery models with noncoherent detection.

In this paper, we will adopt the nonlinear battery models as in [16] and [19] to compare different modulation schemes. We will compare PPM with ON–OFF keying (OOK) since both of them are pulse-based modulations. With PPM and OOK, it is possible to employ carrierless signaling and/or noncoherent reception bypassing channel estimation at the receiver. In our earlier work [15], we compared the BPEs of PPM and OOK based on the exact bit error rate (BER) and the cutoff rate over path-loss additive white Gaussian noise (AWGN) channels. In this paper, we will explore the BPEs of PPM and OOK over Rayleigh fading channels and with varying channel state information (CSI) quality, including both coherent and noncoherent detections.

In our comparisons, we will use the cutoff rate as the criterion, because it takes into account the CSI quality at the receiver. The cutoff rate is a lower bound on capacity that also provides a bound on the random coding exponent [3, pp. 11 and 139–145]. The cutoff rate can also be regarded as a reference for the achievable data rate with an error probability approaching 0 when the length of the randomly selected code approaches infinity [14, Ch. 7]. Further, the cutoff rate is tractable and provides insights that are valuable for practical system designs. Cutoff rate analysis has been commonly adopted since its reintroduction in [10], and studies have been conducted for perfect receiver CSI in [5] and [9], and for no CSI in [4]. Different from these works, [11] gives a universal cutoff rate expression by assuming imperfect CSI at the receiver for binary modulations including OOK. This expression covers both coherent and noncoherent detection. Based on a similar approach, in this work, we will first derive a universal cutoff rate expression for PPM, using which we will compare the BPEs of PPM and OOK under imperfect CSI.

In Section II, we will introduce PPM and duty-cycled OOK modulations, a Rayleigh fading channel with imperfect CSI at the receiver, and the nonlinear battery model. In Section III, we will analyze the cutoff rate of PPM and OOK in terms of the available signal-to-noise ratio (SNR) and CSI quality. Using these results, we will then compare the BPEs in Section IV. Finally, we will give simulation results and concluding remarks in Sections V and VI, respectively.

Manuscript received September 8, 2007; revised March 13, 2008. Published August 13, 2008 (projected). The associate editor coordinating the review of this manuscript and approving it for publication was Dr. Hongbin Li. This work is in part supported by Office of Naval Research under Grant N00014-07-1-0868, and the Army Research Office under Contract W911NF-07-D-0001. Parts of the results in this paper have been presented at Military Communications Conference (MILCOM), Orlando, FL, October 29–31, 2007.

F. Qu, D. Duan, and L. Yang are with the Department of Electrical and Computer Engineering, University of Florida, Gainesville, FL 32611 USA (e-mail: jimqufz@ufl.edu; ddl85@ufl.edu; lqyang@ece.ufl.edu).

A. Swami is with the Army Research Laboratory, Adelphi, MD 20783 USA (e-mail: a.swami@ieee.org).

Digital Object Identifier 10.1109/TSP.2008.924142

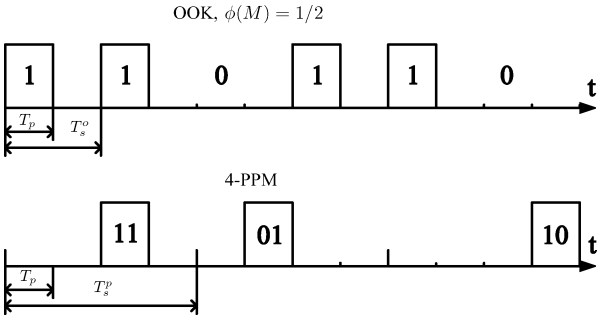

Fig. 1. Baseband waveforms for 4-PPM and OOK with $\phi(M) = 1/2$.

Notation: We will use $\mathbb{E}[\cdot]$ for expectation. Superscripts "p" and "o" refer to PPM and OOK; subscripts "t" and "r" refer to transmitter and receiver; subscripts "s" and "b" represent per symbol and per bit. $x \sim \mathcal{CN}(\mu, \sigma^2)$ denotes a complex Gaussian random variable x with mean μ and variance σ^2.

II. System Model

A. PPM and OOK Modulations

To ensure the same bandwidth occupancy, the pulse duration T_p should be the same for both OOK and PPM. Bandwidth efficiency measured in b/s/Hz is $\log_2(M)/M$ for M-PPM, and T_p/T_s^o for OOK, where T_s^o is the OOK symbol period. To ensure that both OOK and M-PPM have the same bandwidth efficiency, we need $\phi(M) = \log_2(M)/M = T_p/T_s^o$. Here $\phi(M)$ is the duty-cycle, the fractional on-time of the OOK "1" pulse. This implies that, when compared with different PPM modulation sizes M, OOK is duty-cycled with different factors $\phi(M)$; that is, only part of symbol duration is used for transmission. Fig. 1 gives an example of the transmitted waveforms corresponding to 4-PPM and OOK with duty cycle factor $\phi(4) = \log_2 4/4 = 1/2$, both having the same bandwidth occupancy and bandwidth efficiency.

B. Channel Model

We consider a flat-fading Rayleigh channel with path-loss effects. With a path-loss parameter $K > 1$, the channel gain factor $G(d)$ depends on the transceiver distance (communication range) d and is given by [17, Ch. 4]

$$G(d) = \frac{\mathcal{P}_{\rm t}}{\mathcal{P}_{\rm r}} = \frac{\mathcal{E}_{\rm st}}{\mathcal{E}_{\rm sr}} = M_l d^K G_1 \tag{1}$$

where $\mathcal{P}_{\rm t}$ and $\mathcal{P}_{\rm r}$ are the transmitted and received power, $\mathcal{E}_{\rm st}$ and $\mathcal{E}_{\rm sr}$ are the transmitted and received symbol energy, M_l is the link margin and G_1 is the gain factor at $d = 1$. With a transmitted signal $\sqrt{\mathcal{E}_{\rm st}} s_k$ where s_k is the energy normalized symbol, the received signal y_k is given by

$$y_k = \frac{1}{\sqrt{G(d)}} h_k \cdot \sqrt{\mathcal{E}_{\rm st}} s_k + n_k = \sqrt{\mathcal{E}_{\rm sr}} h_k s_k + n_k \tag{2}$$

where k denotes the discrete time index, $h_k \sim \mathcal{CN}(0,1)$ models the independent and identically distributed (i.i.d.) channel fading with unit variance, and $n_k \sim \mathcal{CN}(0, \sigma_N^2)$ models the AWGN.

At the receiver, an estimate of the channel coefficient h_k is obtained as $\hat{h}_k$ during each symbol interval, with residual error $\tilde{h}_k = h_k - \hat{h}_k$. As in [11], we assume that the estimate and the residual error are zero-mean complex Gaussian and mutually independent; that is, $\hat{h}_k \sim \mathcal{CN}(0, \hat{\sigma}^2)$, $\tilde{h}_k \sim \mathcal{CN}(0, \tilde{\sigma}^2)$, and $\hat{\sigma}^2 + \tilde{\sigma}^2 = 1$.[1] Based on these assumptions, $\hat{\sigma}^2$ essentially captures the CSI quality at the receiver. Note that $\hat{\sigma}^2 = 0$ implies no CSI, while $\hat{\sigma}^2 = 1$ indicates perfect CSI.

C. Nonlinear Battery Model

Ideally, the instantaneous power consumption of the battery is $P(i) = Vi$, where V is the battery voltage and i is the discharge current. In [12] and [16], experimental results show that the battery power consumption is a nonlinear process. In this case, the instantaneous power consumption is $P(i) = Vi/\mu(i)$ where $\mu(i) \in [0.5, 1)$ is the battery power efficiency

$$\mu(i) = 1 - \omega i \text{ or } \mu(i) = 1 - \nu i^2 \tag{3}$$

where $\omega > 0$ and $\mu > 0$ are constants extracted from experiments [16]. As a result, the battery power efficiency decreases as the battery discharge current increases.

Unlike OOK, which is always binary, PPM is an M-ary scheme whose symbol energy is concentrated in $1/M$ portion of the symbol period. Therefore, as the modulation size of PPM increases, the symbol energy will be more concentrated in a shorter active portion and the current will be increasingly spiky. This, together with (3), gives rise to a decreasing battery power efficiency. With a linear battery model, however, the extra power loss due to the spiky current of the PPM is not accounted for.

III. Cutoff Rate Analysis Under Imperfect CSI

The cutoff rate R_0 is a lower bound on capacity that also provides a bound on the random coding exponent via $P_e(N) \leq 2^{-N(R_0 - R)}$, where R is the data rate, and $P_e(N)$ is the probability of decoding error for length-N codewords [3, pp. 11 and 139–145], [18]. Let $\boldsymbol{s} = (s_1, s_2, \ldots, s_N)$ denote a transmitted codeword, $\boldsymbol{y} = (y_1, y_2, \ldots, y_N)$ the corresponding received signal and $\hat{\boldsymbol{h}} = (\hat{h}_1, \hat{h}_2, \ldots, \hat{h}_N)$ the channel estimate during the span of the codeword. The decoder treats $\boldsymbol{s}$ as the channel input and the pair $(\boldsymbol{y}, \hat{\boldsymbol{h}})$ as the channel output. By maximizing the posteriori probability of the channel output, the soft-decision maximum *a posteriori* (MAP) decoder yields the following estimate: $\hat{\boldsymbol{s}} = \arg\max_{\boldsymbol{s} \in \mathcal{Q}} P(\boldsymbol{y}, \hat{\boldsymbol{h}} | \boldsymbol{s})$, where $\mathcal{Q}$ is the set of all possible length-N input sequences. Next, in preparation for the battery efficiency comparisons, we will first summarize the cutoff rate of OOK in [11] and then derive the cutoff rate of PPM based on this soft-decision MAP decoder in the presence of imperfect CSI.

[1] A minimum mean-square-error (MMSE) channel estimator satisfying these assumptions can be found in [16, Ch. 11.4].

A. Cutoff Rate of OOK With Imperfect CSI

Under the channel model we described in Section II-B, the cutoff rate for OOK modulation with imperfect CSI was obtained in [11]:

$$R_0^o(q) = -\log_2\left\{1+2q(1-q)\left[\frac{4\sqrt{1+(1-\hat{\sigma}^2)\frac{\gamma}{q}}}{4+2\frac{\gamma}{q}-\hat{\sigma}^2\frac{\gamma}{q}}-1\right]\right\} \tag{4}$$

where $\gamma := \mathcal{E}_{br}/\sigma_N^2$ is the average SNR per bit, $\mathcal{E}_{br}$ is the received energy per bit and q is the probability of transmitting symbol "1".[2] Notice that, due to the duty-cycling factor $\phi(M)$, the unit of the cutoff rate $R_0^o(q)$ given by (4) is not bits/s/Hz, but bits$/T_s^o/B$, which we term as "bits per OOK channel use." To facilitate the comparison between the two modulation formats, we will adopt this unit for the cutoff rate of PPM as well. This will entail some normalization, which we will detail later as needed.

Maximizing the cutoff rate of OOK by numerical search, an optimum q can be obtained [11]:$q^* = \arg\max_{q\in(0,0.5]} R_0^o(q)$. As shown in [11, Fig. 3], q^* is close to 0 at low SNR and approaches 0.5 as SNR increases. In addition, the value of q^* at fixed SNR also increases as the CSI quality improves, resulting in increasing cutoff rates.

B. Cutoff Rate of PPM With Imperfect CSI

As an equi-energy M-ary orthogonal modulation, PPM's cutoff rate is maximized by equi-probable inputs [14, Ch. 7]. In this case, the MAP decoder becomes a maximum-likelihood (ML) decoder. The cutoff rate of M-ary orthogonal modulations with a soft-decision ML decoder was obtained for AWGN channels as [14, Ch. 7]

$$\breve{R}_0 = \log_2 M - \log_2\left\{1+(M-1)\left[\int_y \sqrt{p_{s+n}(y)\cdot p_n(y)}dy\right]^2\right\},$$

measured in bits per PPM channel use ($bits/T_s^p/B$), and with $p_{s+n}(y)$ and $p_n(y)$ denoting the pdfs of $y \sim \mathcal{CN}(\sqrt{\mathcal{E}_{rs}}, \sigma_N^2)$ and $y \sim \mathcal{CN}(0, \sigma_N^2)$, respectively. Using this result, we obtain the cutoff rate of PPM with imperfect CSI as

$$\breve{R}_0^p = \log_2 M - \log_2\{1+(M-1) \times \left[\int_y\int_{\hat{h}} \sqrt{p_{s+n}(y,\hat{h})\cdot p_n(y,\hat{h})}d\hat{h}dy\right]^2\}. \tag{5}$$

Evaluating (5), we establish the following result.

Lemma 1: With imperfect CSI, the cutoff rate of M-ary PPM, measured in bits per OOK channel use, is given by

$$R_0^p = 1-\log_M\left\{1+\frac{16(M-1)\left[\gamma(1-\hat{\sigma}^2)\log_2 M+1\right]}{\left[\gamma(2-\hat{\sigma}^2)\log_2 M+4\right]^2}\right\} \tag{6}$$

[2]In [11], ω is used to denote the CSI quality $\hat{\sigma}^2$, p for OOK probability q, and κ for SNR γ.

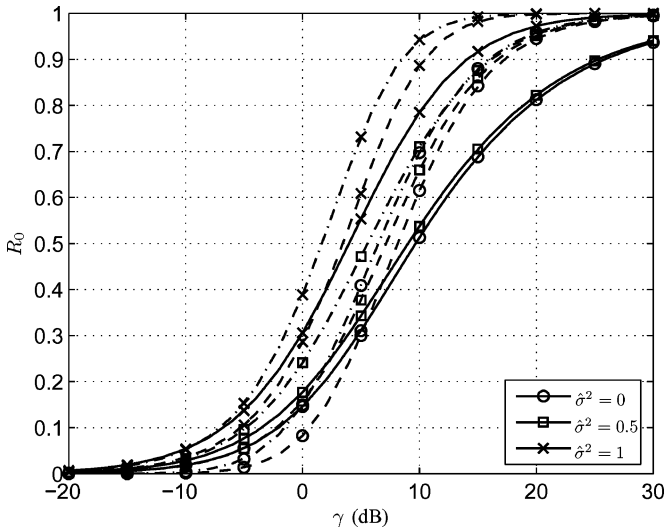

Fig. 2. Cutoff rate versus SNR: Solid curves for OOK, dashed for 2-PPM, and dotted–dashed for 4-PPM.

where $0 \le \hat{\sigma}^2 \le 1$ captures the CSI quality and γ is the SNR per bit.[3]

Proof: See Appendix I. ■

R_0^p has several interesting properties:

P1) For any modulation size M, and with any CSI quality, we always have $0 < R_0^p < 1$. As SNR approaches infinity, R_0^p approaches 1 and when SNR approaches 0, R_0^p approaches 0.

Proof: See Appendix II. ■

The numerical plots in Fig. 2 verify this property for $M = 2$ and $M = 4$ with varying CSI quality.

P2) The cutoff rate R_0^p increases as the CSI quality improves for any modulation size M and SNR values.

Proof: See Appendix III. ■

P3) For small M, the cutoff rate R_0^p increases as M increases. For large M, the cutoff rate R_0^p decreases as M increases.

Proof: See Appendix IV. ■

We proved that the cutoff rate increases when M increases from 2 to 4 in Appendix IV, regardless of the SNR and the CSI quality; we also showed that the cutoff rate decreases with M when M is large. Is this unimodal in M? We do not have a rigorous proof, but Fig. 3 indicates that this might be the case. It also indicates that the maximum value lies in the range 2^3 to 2^5. In any case, there is an M^* that maximizes the cutoff rate.

C. Cutoff Rate Comparison Between PPM and OOK Under Imperfect CSI

From the preceding analysis, we learnt that both PPM and OOK have cutoff rates approaching 1 as the SNR approaches infinity, regardless of the CSI quality. This is reasonable since PPM and OOK can both exploit noncoherent detection even when no CSI is available at the receiver. When the CSI quality reduces from perfect to none, the detection scheme changes from coherent to noncoherent. Using noncoherent detection,

[3]In fact, Lemma 1 applies to general equi-energy orthogonal modulations.

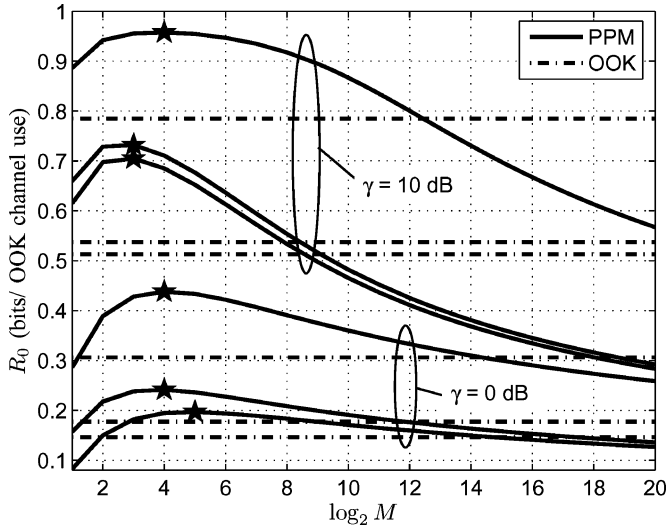

Fig. 3. Cutoff rate with different modulation sizes. For each group, from top to bottom: (1) $\hat{\sigma}^2 = 1$; (2) $\hat{\sigma}^2 = 0.5$; and (3) $\hat{\sigma}^2 = 0$. The stars indicate M^*.

one may still get a sufficiently small BER with a sufficiently high SNR. For other modulations (e.g., binary phase shift keying) which do not facilitate noncoherent detection, the cutoff rate approaches 0 when $\hat{\sigma}^2$ becomes 0, regardless of the SNR [11]. This is an important motivation for us to consider PPM and OOK in this paper.

Though PPM and OOK can both cope with varying CSI qualities, it would be interesting to see how differently they are affected by the CSI quality, the SNR and the PPM modulation size. Evaluating and comparing the cutoff rates for PPM and OOK, the following observations can be obtained:

1a) *For PPM with small modulation sizes, there exists a critical SNR value* $\gamma_c(\hat{\sigma}^2)$ *such that when* $\gamma < \gamma_c(\hat{\sigma}^2)$, $R_0^p < R_0^o(q^*)$, *and when* $\gamma > \gamma_c(\hat{\sigma}^2)$, $R_0^p > R_0^o(q^*)$. These can be observed from the square-marked curves $(M = 2)$ in Fig. 4. Notice that these curves start from $r = R_0^o(q^*)/R_0^p$ with values greater than one, cross $r = 1$ line once and remain at values smaller than one. The SNR at which $r = 1$ is what we term as "critical SNR" $\gamma_c(\hat{\sigma}^2)$. The critical SNR values versus the CSI quality are plotted in Fig. 5 for $M = 2$, 4, 8, 16, and 32. In the area below each curve, the cutoff rate of OOK exceeds that of PPM, and vice versa. From this figure, we can see that as the CSI quality gets better, the critical SNR decreases at the beginning. However, as the CSI quality further increases and approaches perfect CSI, the critical SNR flattens and even increases slightly. In addition, for any fixed CSI quality, the critical SNR $\gamma_c(\hat{\sigma}^2)$ is a monotonically increasing function of the PPM modulation size $M, \forall M \leq M^*$. This monotonicity can be explained by Property P3) in Section III-B.

1b) *For larger modulation sizes, the cutoff rate of PPM is smaller than that of OOK over a small range of SNR, and greater than that of OOK for other SNR values*. As shown by curves without markers $(M = 2^{10})$ in Fig. 4, the behavior of $r = R_0^o(q^*)/R_0^p$ versus γ is very different from the case with small M values. This can be partly explained by Property P3) of R_0^p. Recall that, for different γ and $\hat{\sigma}^2$ values, the cutoff rate of PPM reaches its peak and begins to decrease at different modulation sizes (see also Fig. 3).

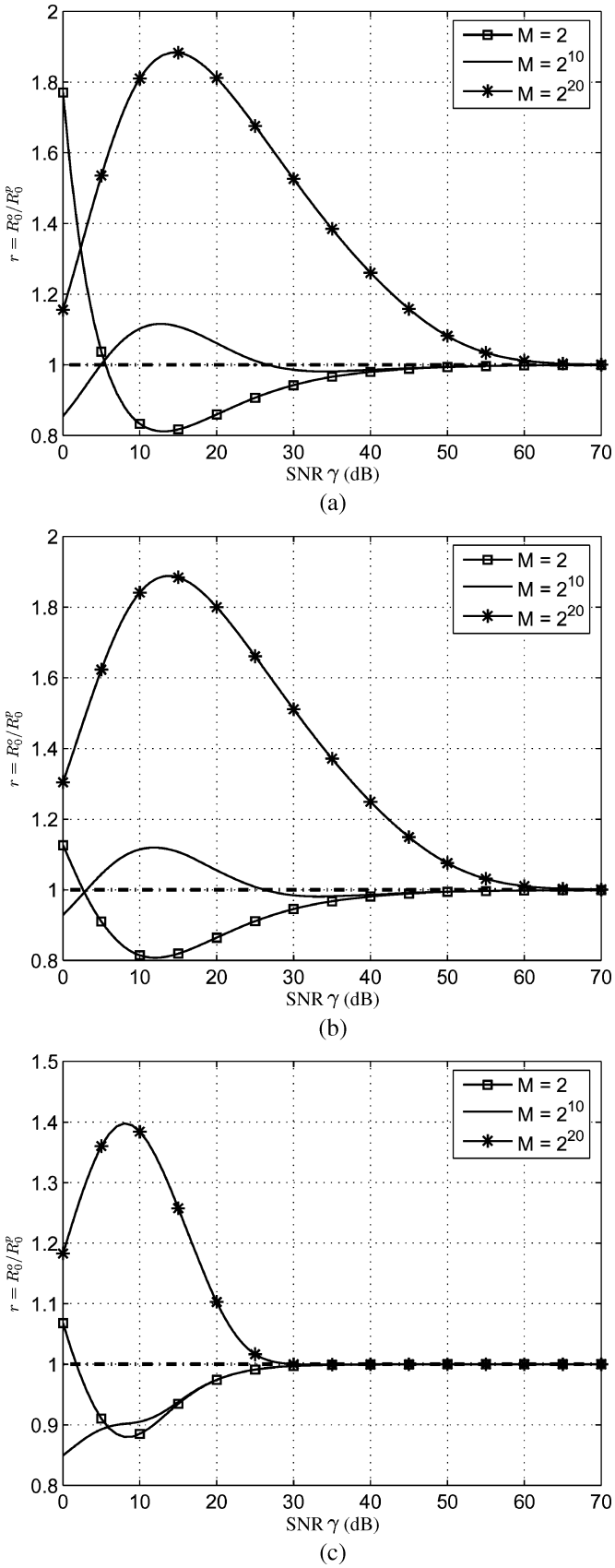

Fig. 4. Cutoff rate ratio of OOK (q^*) and PPM with different modulation sizes. (a) $\hat{\sigma}^2 = 0$. (b) $\hat{\sigma}^2 = 0.5$. (c) $\hat{\sigma}^2 = 1$.

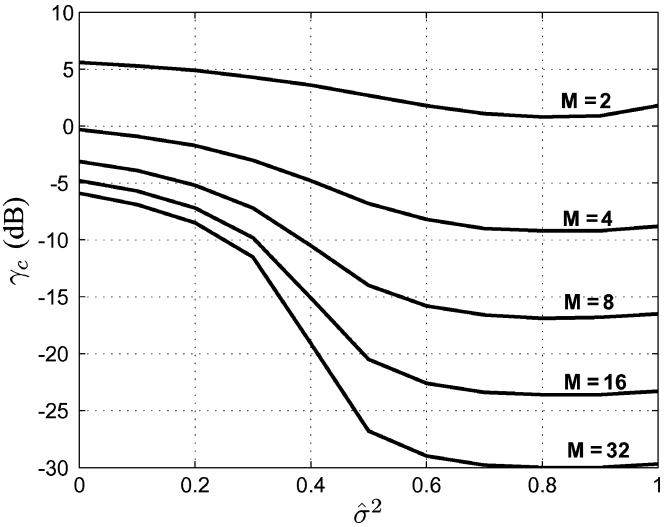

Fig. 5. Critical SNR γ_c with different $\hat{\sigma}^2$. For each curve, M-PPM is better above the curve and OOK is better below.

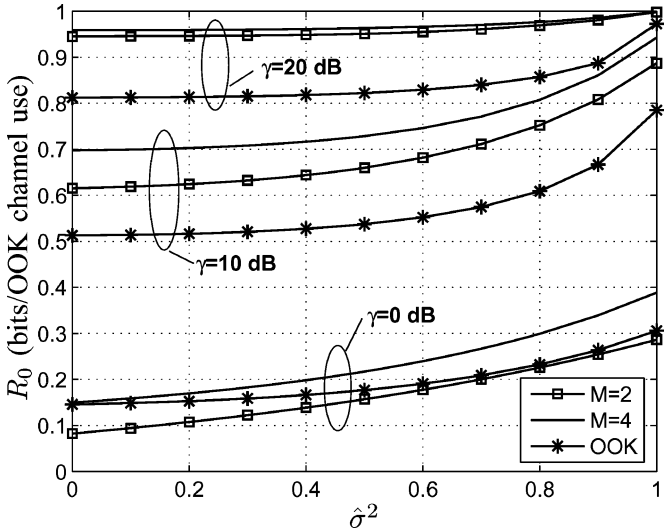

Fig. 6. Cutoff rate of OOK, 2-PPM, and 4-PPM with different CSI quality under different SNRs.

1c) *As the modulation size $M \to \infty$, the cutoff rate of PPM is always smaller than that of OOK.* According to Property P3) of PPM's cutoff rate, and as seen from Fig. 3, R_0^p decreases as M increases when M is large. On the other hand, (4) indicates that the cutoff rate of OOK R_0^o is independent of M (see also Fig. 3). As a result, the cutoff rate of PPM will always fall below that of OOK when the modulation size M is sufficiently large, regardless of γ and $\hat{\sigma}^2$. This is confirmed by the asterisk-marked curves $(M = 2^{20})$ in Fig. 4.

1d) *CSI degradation degrades the cutoff rate more for OOK than PPM at high SNR, and less for OOK than PPM at low SNR.* This can be proved by noticing that

$$\frac{\partial R_0^o}{\partial(\hat{\sigma}^2)} \approx c\frac{\hat{\sigma}^2}{(2-\hat{\sigma}^2)^2}, \quad \text{and} \quad \frac{\partial R_0^p}{\partial(\hat{\sigma}^2)} \approx \frac{c}{\gamma}\frac{\hat{\sigma}^2}{(2-\hat{\sigma}^2)^2}.$$

where c is a constant independent of $\hat{\sigma}^2$. As a result, we have $(\partial R_0^p/\partial(\hat{\sigma}^2)) < (\partial R_0^o/\partial(\hat{\sigma}^2))$ when γ is large, and vice versa.

The impact of imperfect CSI on the cutoff rate of OOK and PPM can be observed from the slope of the curves in Fig. 6. When $\gamma = 20$ dB, as $\hat{\sigma}^2$ becomes worse, the OOK's cutoff rate curve goes down much faster than PPM's cutoff rate curves. At lower SNR, the rates of change of PPM's cutoff rate curves become larger, and the rate of change of OOK's cutoff rate curve becomes slower. At $\gamma = 0$ dB, the rate of change of OOK's cutoff rate curve is smaller than those of PPM's cutoff rate curve. Therefore, we conclude that CSI quality degradation introduces less cutoff rate reduction for OOK than PPM at low SNR.

For orthogonal modulations, it is shown in [14, Ch. 5] that the BER performance difference between coherent and noncoherent demodulators decreases as SNR increases. Hence, the difference between the cutoff rate performance of coherent and noncoherent PPM decoders vanishes as SNR increases, since the cutoff rate is a measure of the average bit error rate. In other words, better CSI quality contributes little to the improvement of PPM's cutoff rate at high SNR, as depicted in the square-marked curves and the curves with no markers with $\gamma = 20$ dB in Fig. 6.

For OOK, however, better CSI quality is essential in precisely determining the threshold for the energy detector, when SNR is high. Accordingly, it improves the cutoff rate performance remarkably, as shown in the asterisk-marked curve with $\gamma = 20$ dB in Fig. 6.

Following this argument at low SNR, we know that for PPM, the performance difference between coherent and noncoherent decoders is large; that is, better CSI quality contributes more to improve PPM's cutoff rate at low SNR. For OOK, though the precise CSI can still help determine the threshold, this threshold is far less effective than in the high-SNR case since the noise is dominant here.

We have seen that theoretically both PPM and OOK can be used to communicate reliably with any CSI quality $\hat{\sigma}^2$. Our analysis has characterized the SNR-CSI regions in which PPM (OOK) should be preferred to OOK (PPM) in terms of cutoff rate (Fig. 5). Fig. 6 also indicates that the cutoff rate (normalized to OOK channel use) increases with CSI quality and modulation size M. In addition, Results 1a)–1d) show that at different SNR levels, PPM modulation sizes and CSI qualities can have very different effects on the relative cutoff rate performance between PPM and OOK.

The analysis so far implicitly assumed that all the power was used for transmission. However, the circuit also consumes power. In addition, as mentioned in Section I, the battery power consumption is nonlinear. In the next section, we will compare the BPEs of PPM and OOK with more realistic battery models.

IV. Battery Power Efficiency Comparison

At energy-constrained WSN nodes, what really matters is not the average transmitted power, but the average actual power consumption (AAPC) that accounts for the circuit power consumption and battery nonlinearity. In particular, the AAPC for OOK at the transmitter is given by [15]

$$\mathcal{P}_{\mathrm{t}}^o = \frac{\log_2 M}{M}\frac{\mathcal{E}^o\beta + q\mathcal{P}_{\mathrm{ct}}}{\eta\mu(I_{\mathrm{t}}^o)} \tag{7}$$

where the subscripts on $\mathcal{E}_{bt}^o$ is dropped for notational simplicity, β is a bandwidth and power amplifier related positive

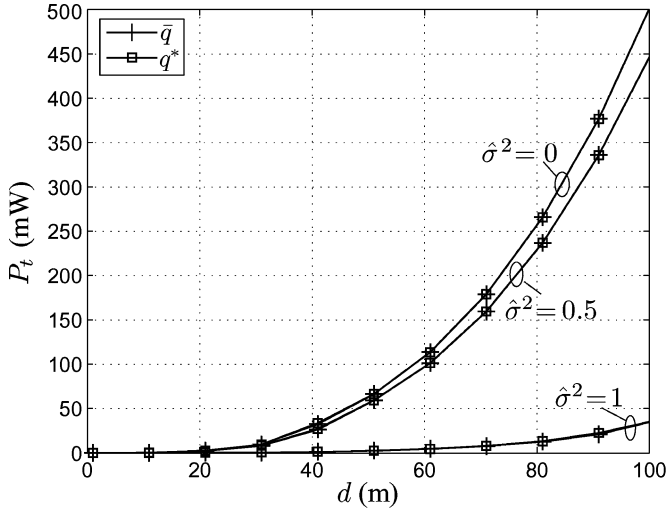

Fig. 7. Power consumption of OOK using q^* and $\bar{q}$.

coefficient, $\mathcal{P}_{\rm ct}$ is the circuit power consumption at the transmitter, $\mu(i)$ is the battery power efficiency we introduced in Section II-C, η is the dc–dc converter efficiency and

$$I_{\rm t}^o = \frac{\beta \mathcal{E}^o/q + \mathcal{P}_{\rm ct}}{V\eta} \tag{8}$$

with V denoting the discharge voltage. Notice that q not only appears explicitly in the numerator of (7), but is also implicitly present in both $\mathcal{E}^o$ and $\mu(I_{\rm t}^o)$. Hence, though q^* minimizes $\mathcal{E}^o$ as discussed in Section III-A, it does not necessarily minimize $\mathcal{P}_{\rm t}^o$ in (7).

In fact, consider the case of large communication range $(d \gg 1)$ where the circuit power can be ignored $(P_{\rm ct} = 0)$. From (7), it follows that

$$\frac{\mathcal{P}_{\rm t}^o(q)}{\mathcal{P}_{\rm t}^o(q^*)} = \frac{\mathcal{E}^o(q)}{\mathcal{E}^o(q^*)} \cdot \frac{\mu(I_{\rm t}^o(q^*))}{\mu(I_{\rm t}^o(q))} > \frac{\mu(I_{\rm t}^o(q^*))}{\mu(I_{\rm t}^o(q))} \quad \forall q$$

where the dependence on q is explicitly shown. The right-hand side of this inequality, however, is a monotonically decreasing function in q and equals 1 when $q = q^*$. In other words, it is possible that $\mathcal{P}_{\rm t}^o(q) < \mathcal{P}_{\rm t}^o(q^*)$ for some $q \in [q^*, 0.5]$. Accordingly, if we term the q value that minimizes $\mathcal{P}_{\rm t}^o$ as $\bar{q}$, then $\bar{q} \in [q^*, 0.5]$ when the circuit power is ignored. However, our simulations show that the resulting difference is negligible (see Fig. 7), and even more so when the circuit power is also included. In addition, the exact value of $\bar{q}$ depends on the actual circuit parameters and may unnecessarily complicate the analysis and comparisons. Therefore, we will use q^* instead of $\bar{q}$ in the sequel.

The node operates in a half-duplex communication mode with $0 < a < 1$ portion of time in the transmitting mode and $(1-a)$ in the receiving mode. As in [15], [19], we adopt the so-termed *battery power efficiency ratio* (BPER) as the comparison metric

$$\rho = 10\log\left[\frac{a\mathcal{P}_{\rm t}^p + (1-a)\mathcal{P}_{\rm r}^p}{a\mathcal{P}_{\rm t}^o + (1-a)\mathcal{P}_{\rm r}^o}\right] \tag{9}$$

where $\mathcal{P}_{\rm t}$ and $\mathcal{P}_{\rm r}$ are the AAPCs at the transmitter and the receiver, respectively. With this definition, PPM is more battery power-efficient if $\rho < 0$ and OOK is more efficient otherwise.

TABLE I
SIMULATION PARAMETERS

$I_{max} = 10$A	$\mathcal{P}_{cr} = 52.5$mW	$G_1 = 27$dB
$V = 3.7$V	$\mathcal{P}_{ct} = 105.8$mW	$M_l = 40$dB
$\omega = 0.05$	$N_0/2 = -171$dBm/Hz	$K = 3$
$a = 0.5$	$\eta = 0.8$	$\beta = 10$kHz

With $\mathcal{P}_{\rm cr}$ denoting the circuit power consumption, and $I_{\rm r}$ the discharge current, both at the receiver, the BPER turns out to be [15]

$$\rho = 10\log\left[\frac{\left(\mathcal{E}^p\beta + \frac{\mathcal{P}_{\rm ct}}{\log_2 M}\right)\frac{1}{\mu(I_{\rm t}^p)} + \frac{M}{\log_2 M}\frac{(1-a)\mathcal{P}_{\rm cr}}{a\mu(I_{\rm r})}}{(\mathcal{E}^o\beta + q\mathcal{P}_{\rm ct})\frac{1}{\mu(I_{\rm t}^o)} + \frac{(1-a)\mathcal{P}_{\rm cr}}{a\mu(I_{\rm r})}}\right] \tag{10}$$

where $I_{\rm t}^p = (\beta\mathcal{E}^p \log_2 M + \mathcal{P}_{\rm ct})/(V\eta)$ is the peak discharge current at the transmitter for PPM and $I_{\rm r} = \mathcal{P}_{\rm cr}/(V\eta)$ is the peak discharge current at the receiver for both modulations.

Now we are ready for the battery power comparison.

2a) *For large modulation size M, OOK is always more battery power-efficient than PPM*. As Property P3) shows, the normalized cutoff rate of PPM decreases with increasing modulation size M. In addition, the nonlinear battery model accounts for the battery efficiency loss introduced by the spiky current of PPM, especially when the modulation size is large.

2b) *For small modulation size M, and with high cutoff rate requirement, PPM is more battery power-efficient than OOK; whereas lower cutoff requirement will reduce the BPE advantage of PPM over OOK*. Result 1a) shows that, at high SNR, to achieve a given cutoff rate R_0, the required SNR for PPM is lower than that for OOK; that is, $\mathcal{E}^p < \mathcal{E}^o$. However, when the required cutoff rate goes down, the system enters the low SNR regime and one will have $\mathcal{E}^p > \mathcal{E}^o$.

2c) *With high cutoff rate requirement* $(R_0 \in [0.5, 1))$, *OOK is more suitable when the CSI quality is good while PPM is more suitable when the CSI quality is bad*. Fig. 2 shows that a high cutoff rate requirement would require both PPM and OOK to have a high SNR. At high SNR, from Result 1d), better CSI quality will contribute to OOK's cutoff rate more than to PPM's. Therefore, better CSI quality will increase the advantage of using OOK, and vice versa.

V. BPER SIMULATION RESULTS

To verify our analysis, we present quantitative results for 2a)–2c). The parameters used in the simulations are shown in Table I [2]. Parameters α, β, η, and $\mu(\cdot)$ are obtained from the power amplifier and battery models, and do not depend upon the modulations. Given distance d, we obtain the path-loss factor $G(d)$ from (1). With a given cutoff rate requirement, for PPM, we get the required SNR directly from the cutoff rate expression; while for OOK, we choose the optimum probability $\bar{q}$ of transmitting a "1" such that the AAPC is minimized and then get the required SNR γ. The average transmitted energy $\mathcal{E}^p$ and $\mathcal{E}^o$ can then be derived from the required SNR. We will also consider different modulation sizes M and CSI qualities $\hat{\sigma}^2$ in our simulations.

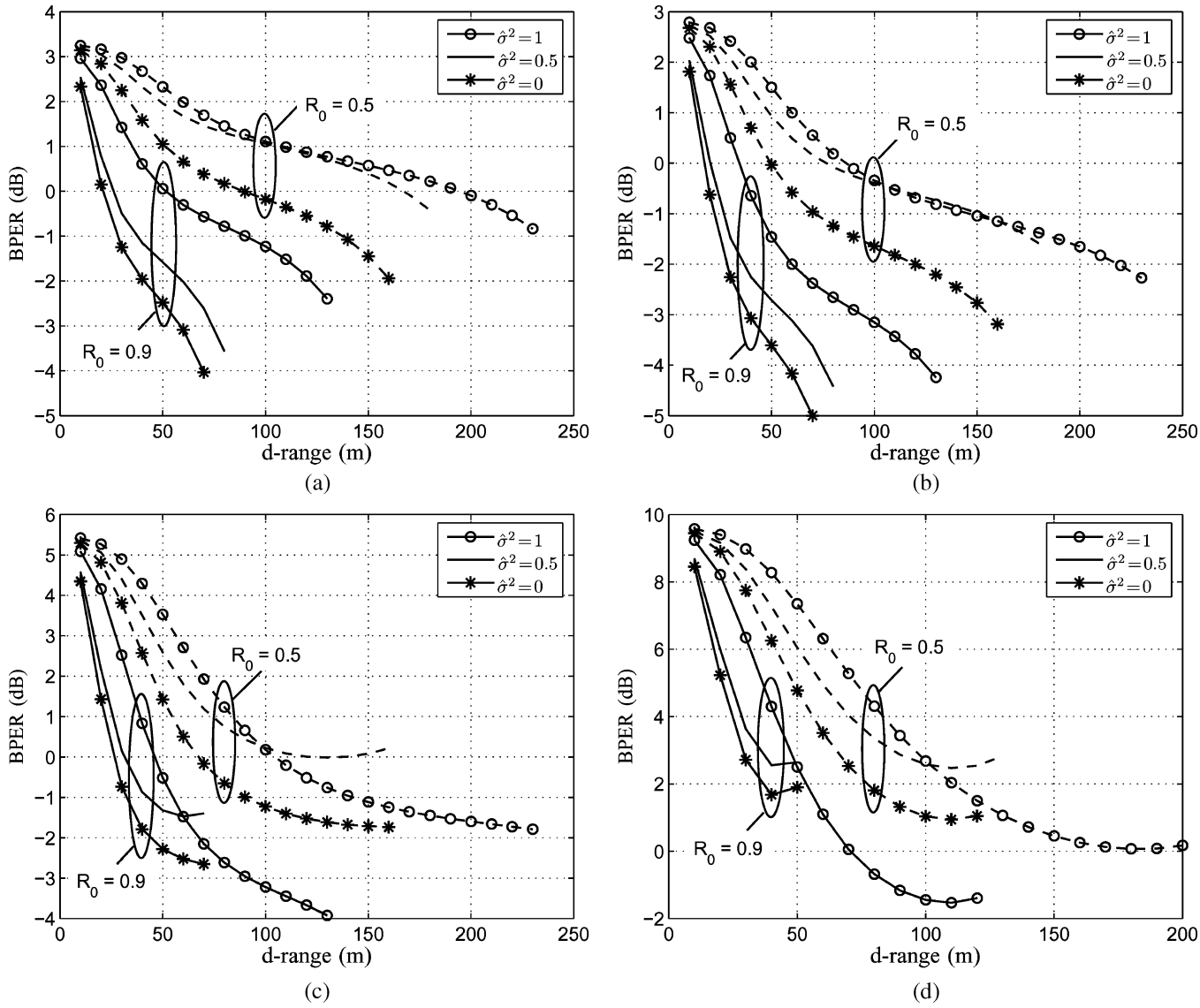

Fig. 8. BPER of M-PPM and OOK versus communication range d. (a) $M = 2$. (b) $M = 4$. (c) $M = 16$. (d) $M = 64$.

Fig. 8 shows the BPER versus communication range d for different modulation sizes M, CSI qualities $\hat{\sigma}^2$ and cutoff rate requirements R_0 combinations with the path-loss exponent $k = 3$. As defined in (9), BPER is the ratio between PPM's power consumption and OOK's power consumption in decibel scale. Thus, the part of curves above 0 means PPM consumes more power, hence OOK is more power efficient, and vice versa.

First, all the curves in these figures go up as the communication range d decreases. This means that OOK outperforms PPM at small communication ranges. This is because, in this case, the circuit power consumption dominates the total battery power consumption. As OOK is duty-cycled and the transceiver circuits are turned off during the idle intervals, OOK will consume less circuit power than PPM.

Comparing the curves with the same $\hat{\sigma}^2$ and R_0 values in Fig. 8, we observe that they are *almost* monotonically increasing as the PPM modulation size increases except for the $M = 2$ case (the order is $M = 4, M = 2, M = 16$, and $M = 64$ from the lowest to the highest BPER curves). This observation is well supported by Property P3) which states that PPM's cutoff rate first increases and then decreases with modulation size M. In addition, when $M = 64$, OOK is nearly always better than PPM since almost all the curves remain above zero. This verifies Result 2a).

For each plot in Fig. 8, the group of curves corresponding to $R_0 = 0.9$ is always below the group corresponding to a lower cutoff rate $R_0 = 0.5$. As predicted by Result 2b), this is because PPM is more battery power efficient at high cutoff rates, but this BPE advantage is reduced as the cutoff rate requirement decreases.

To check the impact of CSI quality on the BPE, we compare the curves within each R_0 group. It is observed that as $\hat{\sigma}^2$ becomes larger, the curve moves upwards, which implies that OOK becomes more battery power efficient relative to PPM, as stated in Result 2c).

VI. Conclusion

We compared the power efficiency of PPM and OOK over flat-fading Rayleigh channels, taking into account imperfect re-

ceiver CSI, and nonlinear battery models, given a desired cutoff rate. First, the cutoff rate of PPM in Rayleigh fading channels with imperfect CSI was derived and compared with that of OOK. We characterized the SNR-CSI quality regions in which OOK (PPM) was preferable to PPM (OOK). We found that with a small modulation size, PPM has higher cutoff rate than OOK at high SNR, while OOK has higher cutoff rate at low SNR. When the modulation size of PPM becomes very large, OOK always outperforms PPM. Then, using realistic nonlinear battery models, the battery power efficiencies of PPM and OOK were compared under the criterion of achieving a desired cutoff rate. The results reveal that PPM with a small modulation size performs better than OOK under high cutoff requirements while OOK is more preferable under low cutoff rate requirements. In addition, OOK is more suitable for shorter communication ranges while PPM is more suitable for longer ones.

APPENDIX I
PROOF OF LEMMA 1

The double integral in (5) can be re-expressed as[4]

$$\int_y \int_{\hat{h}} \sqrt{p_{s+n}(y,\hat{h})\cdot p_n(y,\hat{h})}\,d\hat{h}dy = \mathbb{E}_{\hat{h}}\left[\int_y \sqrt{p_{s+n}(y|\hat{h})\cdot p_n(y|\hat{h})}dy\right]$$

where $p_{s+n}(y|\hat{h})$ is the conditional pdf of $y|\hat{h} \sim \mathcal{CN}(\sqrt{\mathcal{E}_s}\hat{h}, \mathcal{E}_s\tilde{\sigma}^2+\sigma_N^2)$ and $p_n(y|\hat{h})$ is the conditional pdf of $y|\hat{h}\sim\mathcal{CN}(0,\sigma_N^2)$, with $\tilde{\sigma}^2$ the variance of the residual channel estimation error $\tilde{h}$ and σ_N^2 the variance of the complex white Gaussian noise at the receiver. Evaluating with the respective pdf expressions, we get

$$\int_y \sqrt{p_{s+n}(y|\hat{h})\cdot p_n(y|\hat{h})}dy = \frac{2\sqrt{\sigma_N^2\left(\mathcal{E}_s\tilde{\sigma}^2+\sigma_N^2\right)}}{\mathcal{E}_s\tilde{\sigma}^2+2\sigma_N^2} \cdot\exp\left(\frac{-\mathcal{E}_s|\hat{h}|^2}{2\left(\mathcal{E}_s\tilde{\sigma}^2+2\sigma_N^2\right)}\right).$$

Then, we take expectation of the above equation with respect to $\hat{h}\sim\mathcal{CN}(0,\hat{\sigma}^2)$ and obtain

$$\mathbb{E}_{\hat{h}}\left[\int_y \sqrt{p_{s+n}(y|\hat{h})\cdot p_n(y|\hat{h})}dy\right] = \frac{4\sqrt{\sigma_N^2\left(\mathcal{E}_s\tilde{\sigma}^2+\sigma_N^2\right)}}{\mathcal{E}_s\hat{\sigma}^2+2\mathcal{E}_s+4\sigma_N^2}.$$

Substituting the above result into (5), and noticing that for PPM, $\mathcal{E}_b=\mathcal{E}_s/\log_2 M$, $\gamma=\mathcal{E}_b/\sigma_N^2$, we get the cutoff rate for PPM measured in *bits per PPM channel use* as

$$\breve{R}_0 = \log_2 M - \log_2\left\{1+\frac{16(M-1)\left[\gamma(1-\hat{\sigma}^2)\log_2 M+1\right]}{\left[\gamma(2-\hat{\sigma}^2)\log_2 M+4\right]^2}\right\}. \tag{11}$$

To ease its comparison with the cutoff rate of OOK, we convert $\breve{R}_0$, measured in bits per PPM channel use $(bits/T_s^p/B)$, into the R_0, measured in bits per OOK channel use $(bits/T_s^o/B)$. Noticing that $T_s^p=\log_2 M\cdot T_s^o$, the cutoff rate of PPM measured in bits per OOK channel use can be obtained as $R_0=\breve{R}_0/\log_2 M$, which leads to (6) and concludes the proof.

[4]All variables in this section are for PPM, except T_s^o for OOK.

APPENDIX II
PROOF OF PROPERTY P1)

For any $M\geq 2$, it is clear that

$$\frac{16(M-1)\left[\gamma(1-\hat{\sigma}^2)\log_2 M+1\right]}{\left[\gamma(2-\hat{\sigma}^2)\log_2 M+4\right]^2}>0.$$

In addition, it follows from

$$\begin{aligned}\left[\gamma(2-\hat{\sigma}^2)\log_2 M+4\right]^2 &> 8\gamma(2-\hat{\sigma}^2)\log_2 M+16\\ &> 16\left[\gamma(1-\hat{\sigma}^2)\log_2 M+1\right]>0\end{aligned}$$

that

$$\frac{16(M-1)\left[\gamma(1-\hat{\sigma}^2)\log_2 M+1\right]}{\left[\gamma(2-\hat{\sigma}^2)\log_2 M+4\right]^2}<M-1.$$

These prove that $0<R_0^p<1$.

For any modulation size $M>1$, and with any given $\hat{\sigma}^2$, as $\gamma\to\infty$, we have

$$\begin{aligned}&\lim_{\gamma\to\infty}\frac{16(M-1)\left[\gamma(1-\hat{\sigma}^2)\log_2 M+1\right]}{\left[\gamma(2-\hat{\sigma}^2)\log_2 M+4\right]^2}\\ &=\lim_{\gamma\to\infty}\frac{\gamma\cdot 16(M-1)\left[(1-\hat{\sigma}^2)\log_2 M\right]}{\gamma^2\cdot\left[(2-\hat{\sigma}^2)\log_2 M\right]^2}\\ &=0.\end{aligned}$$

As a result, $\lim_{\gamma\to\infty}R_0^p=1$.

Likewise, when $\gamma\to 0$, we have:

$$\lim_{\gamma\to 0}\frac{16(M-1)\left[\gamma(1-\hat{\sigma}^2)\log_2 M+1\right]}{\left[\gamma(2-\hat{\sigma}^2)\log_2 M+4\right]^2}=M-1$$

and, accordingly, $\lim_{\gamma\to 0}R_0^p=0$.

APPENDIX III
PROOF OF PROPERTY P2)

Differentiating R_0^p with respect to the CSI quality $\hat{\sigma}^2$, we have:

$$\begin{aligned}\frac{\partial R_0^p}{\partial(\hat{\sigma}^2)} &= -\frac{\left[\gamma(2-\hat{\sigma}^2)\log_2 M+4\right]^2}{\log_2 M\left[\gamma(1-\hat{\sigma}^2\log_2 M)+1\right]}\\ &\quad\cdot\left[\frac{\partial}{\partial(\hat{\sigma}^2)}\frac{\gamma(1-\hat{\sigma}^2\log_2 M)+1}{\left[\gamma(2-\hat{\sigma}^2)\log_2 M+4\right]^2}\right]\\ &=\frac{\left[\gamma(2-\hat{\sigma}^2)\log_2 M+4\right]^2}{\log_2 M\left[\gamma(1-\hat{\sigma}^2\log_2 M)+1\right]}\\ &\quad\cdot\frac{\gamma\log_2 M(\hat{\sigma}^2\log_2 M+2)}{\left[\gamma(2-\hat{\sigma}^2)\log_2 M+4\right]^3}>0.\end{aligned}$$

Hence, R_0^p increases as $\hat{\sigma}^2$ increases.

APPENDIX IV
PROOF OF PROPERTY P3)

Let us now explicitly denote $R_0^p(M)$ as a function of the PPM modulation size M. From (6), we have

$$R_0^p(4) = 1 - \log_4\left\{1 + 3\frac{16\left[2\gamma(1-\hat{\sigma}^2)+1\right]}{\left[2\gamma(2-\hat{\sigma}^2)+4\right]^2}\right\} = 1 - \log_2\sqrt{1 + 3\frac{16\left[2\gamma(1-\hat{\sigma}^2)+1\right]}{\left[2\gamma(2-\hat{\sigma}^2)+4\right]^2}}.$$

Since R_0^p decreases as the SNR decreases, we have

$$R_0^p(4) > 1 - \log_2\sqrt{1 + 3\frac{16\left[\gamma(1-\hat{\sigma}^2)+1\right]}{\left[\gamma(2-\hat{\sigma}^2)+4\right]^2}}.$$

Further noticing that $\sqrt{1+3x} < 1 + x$ when $0 < x < 1$, we obtain

$$R_0^p(4) > 1 - \log_2\left\{1 + \frac{16\left[\gamma(1-\hat{\sigma}^2)+1\right]}{\left[\gamma(2-\hat{\sigma}^2)+4\right]^2}\right\} = R_0^p(2).$$

Hence, $R_0^p(4) > R_0^p(2)$ for any combinations of γ and $\hat{\sigma}^2$ values; that is, PPM's cutoff rate increases as M increases from 2 to 4.

However, when M is large, we have

$$R_0^p \approx \log_2\left\{\frac{M}{1 + \frac{16M\gamma(1-\hat{\sigma}^2)\log_2 M}{[\gamma(2-\hat{\sigma}^2)\log_2 M]^2}}\right\} \approx \frac{\log_2\log_2 M}{\log_2 M}$$

which is a decreasing function of M.

REFERENCES

[1] I. F. Akyildiz, W. Su, Y. Sankarasubramaniam, and E. Cayirci, "Wireless sensor networks: A survey," *Comput. Netw.*, pp. 393–422, Mar. 2002.

[2] S. Cui, A. J. Goldsmith, and A. Bahai, "Energy-constranined modulation optimization," *IEEE Trans. Commun.*, vol. 4, no. 5, pp. 2349–2360, Sep. 2002.

[3] R. G. Gallager, *Information Theory and Reliable Communication*. New York: Wiley, 1968.

[4] A. O. Hero and T. L. Marzetta, "Cutoff rate and signal design for the quasi-static Rayleigh fading space-time channel," *IEEE Trans. Inf. Theory*, vol. 47, no. 6, pp. 2400–2416, Sep. 2001.

[5] S. Jamali and T. Le-Ngoc, *Coded-Modulation Technique for Fading Channels*. Norwell, MA: Kluwer Publisher, 1994.

[6] S. M. Kay, *Fundamentals of Statistical Signal Processing, Volume I: Estimation Theory*. Englewood Cliffs, NJ: Prentice-Hall, 1993.

[7] K. Lahiri, A. Raghunathan, S. Dey, and D. Panigrahi, "Battery-driven system design: A new frontier in low power design," in *Proc. Int. Conf. VLSI Design*, Bangalore, India, Jan. 7–11, 2002, pp. 261–267.

[8] J. N. Laneman, D. N. C. Tse, and G. W. Wornell, "Cooperative diversity in wireless networks: Efficient protocals and outage behavior," *IEEE Trans. Inf. Theory*, vol. 50, no. 12, pp. 3062–3080, Dec. 2004.

[9] K. Leeuwin-Boulle and J. C. Belfiore, "The cutoff rate of time-correlated fading channels," *IEEE Trans. Inf. Theory*, vol. 39, no. 2, pp. 612–617, Mar. 1993.

[10] J. Massey, "Coding and modulation in digital communications," in *Proc. Int. Zurich Seminar Digital Communications*, Zurich, Switzerland, Mar. 12–15, 1974.

[11] S. Misra, A. Swami, and L. Tong, "Cutoff rate optimal binary inputs with imperfect csi," *IEEE Trans. Wireless Commun.*, vol. 5, no. 10, pp. 2903–2913, Oct. 2006.

[12] M. Pedram and Q. Wu, "Battery-powered digital CMOS design," *IEEE Trans. VLSI Systems*, vol. 10, no. 5, p. 607, Oct. 2002.

[13] Y. Prakash and S. K. S. Gupta, "Energy efficient source coding and modulation for wireless applications," in *Proc. Wireless Communications Networking Conf.*, New Orleans, LA, Mar. 16–21, 2003, pp. 212–217.

[14] J. Proakis, *Digital Communications*, 4th ed. New York: McGraw-Hill, Feb. 2001.

[15] F. Qu, L. Yang, and A. Swami, "Battery power efficiency of PPM and OOK in wireless sensor networks," presented at the Int. Conf. Acoustics, Speech, Signal Processing (ICASSP), Honolulu, HI, Apr. 15–20, 2007.

[16] D. Rakhmatov and S. Vrudhula, "Time to failure estimation for batteries in portable systems," in *Proc. Int. Symp. Low Power Electronics Design*, Huntington Beach, CA, Aug. 6–7, 2001, pp. 88–91.

[17] T. S. Rappaport, *Wireless Communications: Principles and Practice*, 2nd ed. Englewood Cliffs, NJ: Prentice-Hall, 2002.

[18] A. Saleh and J. Salz, "On the computational cutoff rate, R_0, for the peak-power-limited Gausssian channel," *IEEE Trans. Commun.*, vol. 35, no. 1, pp. 13–20, Jan. 1987.

[19] Q. Tang, L. Yang, G. B. Giannakis, and T. Qin, "Battery power efficiency of PPM and FSK in wireless sensor networks," *IEEE Trans. Commun.*, vol. 6, no. 4, pp. 1308–1319, Apr. 2007.

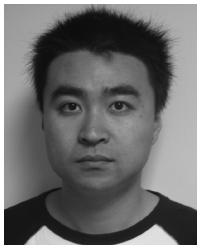

Fengzhong Qu (S'07) received the B.Sc. and M.Sc. degrees from Zhejiang University, Hangzhou, China, in 2002 and 2005, respectively, both in electrical engineering. He is currently working towards the Ph.D. degree with the Department of Electrical and Computer Engineering, University of Florida, Gainesville.

His research interests are in the areas of wireless communications, underwater acoustic communications, and related fields.

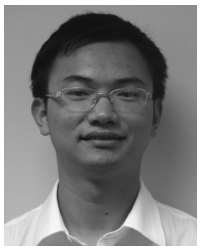

Dongliang Duan (S'07) received the B.S. degree in electrical engineering from Huazhong University of Science and Technology, Wuhan, China, in 2006. He is currently working towards the Ph.D. degree in the Department of Electrical and Computer Engineering at the University of Florida, Gainesville.

His current interests are in the areas of adaptive signal processing in wireless communication and related fields.

Liuqing Yang (S'02–M'04–SM'06) received the B.S. degree in electrical engineering from Huazhong University of Science and Technology, Wuhan, China, in 1994 and the M.Sc. and Ph.D. degrees in electrical and computer engineering from the University of Minnesota, Minneapolis, in 2002 and 2004, respectively.

Since August 2004, she has been an Assistant Professor with the Department of Electrical and Computer Engineering at the University of Florida, Gainesville. Her current research interests include signal processing, communications theory, and networking.

Dr. Yang received the Best Dissertation Award in the Physical Sciences and Engineering from the University of Minnesota in 2005, and the Office of Naval Research Young Investigator Award in 2007. She is the corecipient of the Best Paper Award at IEEE international Conference on UWB (ICUWB) in 2006. She serves as an Associate Editor of the IEEE TRANSACTIONS ON COMMUNICATIONS, the IEEE TRANSACTIONS ON WIRELESS COMMUNICATIONS, and the IEEE TRANSACTIONS ON INTELLIGENT TRANSPORTATION SYSTEMS. She is also a member of the Editorial Board of *Signal, Image and Video Processing Journal*, and *PHYCOM: Physical Communication*. She has been the Co-Chair of the Mobile Communication Networks Technical Committee of the IEEE ITSS since 2006. She was the secretary of the IEEE Gainesville section from 2006 to 2007, and now serves as the Vice-Chair.

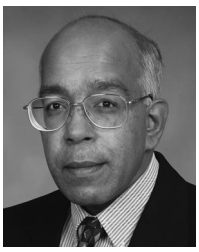

Ananthram Swami (SM'96–F'08) received the B.Tech. degree from the Indian Institute of Technology (IIT)—Bombay; the M.S. degree from Rice University, Houston, TX; and the Ph.D. degree from the University of Southern California (USC), Los Angeles, all in electrical engineering.

He has held positions with Unocal Corporation, USC, CS-3, and Malgudi Systems. He was a Statistical Consultant to the California Lottery, developed a Matlab-based toolbox for non-Gaussian signal processing, and has held visiting faculty positions at INP, Toulouse, France. He is currently with the U.S. Army Research Laboratory, where his work is in the broad area of signal processing, wireless communications, and sensor and mobile ad hoc networks. He is a Co-Editor, with Q. Zhao, Y.-W. Hong, and L. Tong, of the book *Wireless Sensor Networks: Signal Processing & Communications Perspectives* (Wiley, 2007).

He has served as an Associate Editor of the IEEE TRANSACTIONS ON WIRELESS COMMUNICATIONS, IEEE SIGNAL PROCESSING LETTERS, the IEEE TRANSACTIONS ON CIRCUITS & SYSTEMS II, the *IEEE Signal Processing Magazine*, and the IEEE TRANSACTIONS ON SIGNAL PROCESSING. He was Co-Guest Editor of a 2004 Special Issue of the *IEEE Signal Processing Magazine* on Signal Processing for Networking, a 2006 *IEEE Signal Processing Magazine* Special Issue on Distributed Signal Processing in Sensor Networks, a 2006 *EURASIP Journal on Advances in Signal Processing* Special Issue on Reliable Communications over Rapidly Time-Varying Channels, a 2007 *EURASIP Journal on Wireless Communications and Networking* Special Issue on Wireless Mobile Ad Hoc Networks, and is the Lead Editor for a 2008 IEEE JOURNAL ON SELECTED TOPICS IN SIGNAL PROCESSING Special Issue on Signal Processing and Networking for Dynamic Spectrum Access.